bradscholars

Preparation of flexible polymer sensor material by Spatial Confining Forced Network Assembly Micro Injection Molding

Item Type	Article
Authors	Wang, X.;Zhou, S.;Whiteside, Benjamin R.;Wang, J.;Huang, Y.;Xu, H.;Sun, J.;Wu, D.;Coates, Philip;Gao, X.
Citation	Wang X, Zhou S, Whiteside B et al (2024) Preparation of flexible polymer sensor material by Spatial Confining Forced Network Assembly Micro Injection Molding. IEEE Sensors Journal. 24(24): 41777-41786.
DOI	https://doi.org/10.1109/JSEN.2024.3477733
Rights	© 2024 IEEE. Personal use of this material is permitted. Permission from IEEE must be obtained for all other uses, in any current or future media, including reprinting/republishing this material for advertising or promotional purposes, creating new collective works, for resale or redistribution to servers or lists, or reuse of any copyrighted component of this work in other works.
Download date	2025-12-09 07:58:29
Link to Item	http://hdl.handle.net/10454/20169

Preparation of flexible polymer sensor material by Spatial Confining Forced Network Assembly Micro Injection Molding

Xiaojie Wang, Shuangquan Zhou, Ben Whiteside, Junyi Wang, Yao Huang, Hong Xu, Jingyao Sun, Daming Wu, Phil Coates*, Xiaolong Gao*

***Abstract*—The development of high-performance flexible pressure-sensing materials necessitates the simultaneous achievement of exceptional flexibility, conductivity, and alignment of micro-nano structures with the mechanical response characteristics inherent to these materials. In this study, we propose a novel method for preparing flexible microneedles as a pressure-sensitive sensor array. Firstly, we obtain conductive composite particles through extrusion granulation, which consists of a compact conductive network with micron-scale filler as the skeleton and nano-filler filling in the gaps within the network. Moreover, by utilizing the 'volume exclusion' effect of the microneedle array on the micron-scale filler during injection molding, nanofillers dominate in entering the microneedle. As a result, our molded product exhibits high flexibility and moderate conductivity in its pressure-sensitive area, thereby providing ultra-high-pressure resistance along with desired response characteristics and sensitivity for sensors. Additionally, due to synergistic effects between microscale fillers and nano-fillers in non-pressure sensitive bases, a compact conductive network is formed that imparts sufficient conductivity to sensor materials. The method yields sensors with excellent repeatability, high dimensional accuracy, and good consistency, effectively addressing core application challenges of flexible sensors. The microstructure array flexible sensor fabricated using high-precision injection molding technology offers high efficiency, low cost, and scalability for mass production. Furthermore, the sensitivity of sensors produced by this method is significantly higher—26.6% greater than those made using traditional methods—with a sensitivity as high as 4.71kPa^{-1}**

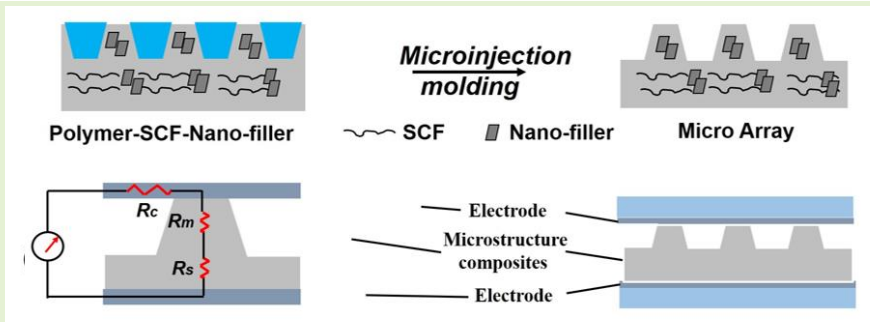

***Index Terms*—Forming, Injection moulding, Multifunctional composites, Carbon nanotubes and nanofibers**

I. INTRODUCTION

In recent years, the research focus has shifted towards flexible pressure sensors due to their unique characteristics [1-3]. There is an urgent need to develop a novel type of low-cost and high-performance flexible pressure sensor that can be widely utilized. Researchers have discovered that incorporating microstructure into the pressure-sensitive unit of the sensor significantly enhances its sensitivity and response time [13-20]. By applying microstructure treatment to either the dielectric or conductive layer of the sensor, not only can deformation be increased, but also higher sensitivity and faster response time can be achieved compared to unstructured sensors [4]. Currently employed microstructures include pyramids, micro-dots, concave and convex patterns [5-7]. The pyramid microstructure-based sensor exhibits a 30-fold improvement in pressure sensitivity compared to unstructured counterparts

Manuscript received 23 May 2024; Corresponding author: Phil Coates and Xiaolong Gao.
Xiaojie Wang is with the School of Mechanical and Electrical Engineering, Beijing University of Chemical Technology, Beijing 100020, China(e-mail: wxj_buct@163.com).
Shuangquan Zhou is with the School of Mechanical and Electrical Engineering, Beijing University of Chemical Technology, Beijing 100020, China(e-mail: zsq20210620@163.com).
Ben Whiteside is now with the Polymer IRC, University of Bradford, Bradford, BD7 1DP, UK(e-mail: B.R.Whiteside@bradford.ac.uk).
Junyi Wang is with the School of Mechanical and Electrical Engineering, Beijing University of Chemical Technology, Beijing 100020, China(e-mail: 2023210419@mail.buct.edu.cn).
Yao Huang is now with the College of Mechanical and Electrical Engineering, Beijing University of Chemical Technology, Beijing 100029, China(e-mail: hy06@163.com)
Hong Xu is now with the College of Mechanical and Electrical Engineering, Beijing University of Chemical Technology, Beijing 100029, China(e-mail: xuhong@mail.buct.edu.cn)
Jingyao Sun is now with the College of Mechanical and Electrical Engineering, Beijing University of Chemical Technology, Beijing 100029, China(e-mail: sunjingyao@mail.buct.edu.cn)
Daming Wu is now with the College of Mechanical and Electrical Engineering, Beijing University of Chemical Technology, Beijing 100029, China(e-mail: wudaming@vip.163.com)
Phil Coates is now with the Polymer IRC, University of Bradford, Bradford, BD7 1DP, UK(e-mail: P.D.Coates@bradford.ac.uk).
Xiaolong Gao is now with the College of Mechanical and Electrical Engineering, Beijing University of Chemical Technology, Beijing 100029, China(e-mail: gao-xl@qq.com)

XXXX-XXXX © XXXX IEEE. Personal use is permitted, but republication/redistribution requires IEEE permission.
See http://www.ieee.org/publications_standards/publications/rights/index.html for more information.

while maintaining a response time within the milliseconds (ms) range.

Among them, the template method is subdivided into silicon template method and AAO template method, and the silicon template method plays an increasingly important role in the preparation of flexible pressure sensors. Silicon template method is to prepare different microstructure array templates through photolithography and other techniques, and then use the template to prepare flexible sensors with microstructures. The microstructures prepared by the photolithographic template method have a good and uniform distribution, which results in higher sensitivity. Cheng Wenlong [8] prepared three different microstructured arrays of PDMS films using the silicon template method, and finally the prepared polymer films were laminated into a sandwich structure. The prepared sensors have a high sensitivity of 23 kPa^{-1} and a fast response time of 10 ms at low pressures (<600 pa) and good stability over 10,000 operating cycles. Silicon template method can effectively improve the performance of the sensor, and low cost, large production scale, and a wide range of applications, but the template is not disposable, and the integrity of the microstructure in the later stage will be affected after many times of use, which in turn affects the performance of the sensor. In order to improve the problem of microstructural incompleteness of the silicon template method, researchers proposed the Anodic Aluminum Oxide (AAO) method, which is a synthetic method to control, influence and modify the morphology of the material by taking the porous anodic aluminium oxide film as the main conformation to control the dimensions and thus determine the properties of the material. The AAO template method uses etching solution to dissolve the AAO template directly, which can be effectively used for the production of sensors. The AAO template method directly uses etching solution to dissolve the AAO template, which can effectively ensure the homogeneity and integrity of the micro-nanostructure, and thus significantly improve the stability of the sensor [9]. Gui Xu-Chun et al [10] prepared a WG/AAO/WG-based sandwich structure flexible sensor using two nanoscale pleated graphene films, which had a sensitivity of 6.29 kPa^{-1} and a cyclic stability of 10,000 cycles in the pressure range of 300 Pa-1.5 kPa. Yang Li [11] also prepared a double-sided nanopillar-structured capacitive pressure sensor by the AAO template method, and the prepared sensor has a high sensitivity (0.35 kPa^{-1}) as well as an extremely wide operating range (4-25 kPa^{-1}) with a short response time (48 ms) and a good cycling stability (3000 cycles). Youdi Hu [16] combined the AAO templating method with the silicon templating method to prepare a silver- and fluoroalkyl-modified hierarchical armoured substrate (Ag/F-HA) with a bi-layer stacked design, where the micro-armour structure was made by femtosecond laser machining to act as a super-hydrophobic and low-adhesion surface to concentrate the analyte, and anodized aluminium oxide (AAO) templates to form nanopillar arrays that act as densely ordered hot spots. With the synergistic effect of hotspots and analyte concentration, the detection limit of Ag/F-HA was as low as 10~7M molecules of adriamycin (DOX) with an RSD of 7.69%. The AAO template method is used to prepare flexible microarray sensors with excellent sensing performance, which can effectively reduce the production cost and realise mass production, but the pressure sensors prepared by the AAO template method have a small measuring pressure range due to the limited deformation of the microstructure. To further improve the performance of the sensors, researchers have found inspiration from nature and used bionic techniques to mimic microstructures in nature. Chuanfei Guo [12] constructed a highly sensitive flexible sensor with high sensitivity (1.2 kPa^{-1}), ultra-low detection limit (<0.8 Pa), and fast response time (36 ms) by using a bionic micropatterned polydimethylsiloxane (m-PDMS) replicated from a lotus leaf. Lan-yen Liu [13] replicated the micro-bump structure on the surface of rose petals on the surface of PDMS by a two-step replication method, and the sensor exhibited high sensitivity (1.35 kPa^{-1}), very low detection limit (2 Pa), short response hysteresis time (30 ms), and excellent cyclic operating stability (5000 cycles). The presence of randomly distributed nanostructures in the microstructures prepared by the bionic method greatly enhances the sensing performance of the flexible pressure sensors compared to the conventional template method and the AAO template method. Although the biomimetic template method has unique advantages in terms of cost and process, the microstructural arrays on the surface still show a relatively more regular distribution to some extent. Meanwhile, for the microarray sensor devices constructed by the natural biotemplate method, its controllable morphology and large-volume reproducible production are still difficult to achieve. In order to solve the above problems, researchers have carried out a lot of explorations. Inspired by the human skin hair structure, the surface of such irregular and randomly distributed high aspect ratio cilia structures can provide a large specific surface area, which greatly increases the saturation of the structural deformation. The magnetron method, as one of the microcilia array structure construction methods, has been widely investigated in recent years due to its simplicity and ease of control, and a large number of research groups have utilised this method to prepare high-performance flexible microarray pressure sensors that can be applied in various fields. Zhou Bingpu [14] constructed a high-sensitivity flexible sensor regulated by the microstructure of the dielectric layer based on the magnetron method, which has a high sensitivity of 0.28 kPa^{-1} in the range of 0-10 kPa, a maximum detection range of up to 200 kPa, and can detect a very small stress of 2 Pa, and maintains a stable response within 10,000 duty cycles. Zhou Bingpu [15] used the magnetron method to design a composite elastic dielectric consisting of low dielectric microcilia arrays and high dielectric rough surface and microdome arrays, based on the composite dielectric structure of the sensor can be up to 1,000kPa in the ultra-wide pressure range to maintain a high sensitivity of 0.314kPa^{-1}. The basic electrical characteristics of the flexible pressure sensors from different preparation processes are shown in Table 1.

Table 1: Basic electrical characteristics of the flexible pressure sensors from different preparation processes

Preparation method	sensitivity /kPa^{-1}	durability /cycle	Test Pressure Range /kPa	response time /ms	reference
Silicon template method	23	10000	<0.6	10	8
AAO	6.583	10000	0-1	36	9
	6.29	10000	0.3-1.5	-	10
	0.35	3000	0.004-25	48	11
biomimetic template method	1.2	-	<0.0008	36	12
	0.35	5000	<0.002	30	13
Magnetic field control method	0.28	10000	0-10	-	14
	0.314	-	1000	-	15

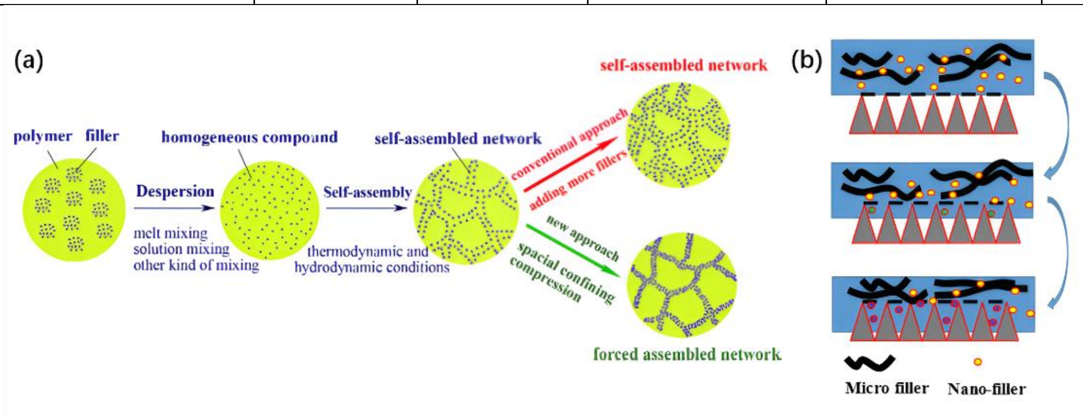

Fig. 1. (a) Comparison between space-restricted forced assembly method and self-assembly method (b) Volume exclusion method

The conductive network structure plays a dominant role in the performance of resistance strain sensors. Currently, three main methods are employed to establish such regularity in the conductive path variation [20-25]. Among these approaches, the filler self-assembly method is widely adopted due to its broad applicability across various material systems as well as its simplicity and equipment versatility. However, when using this self-assembly mode, reaching the dispersion threshold leads to an increased volume fraction of fillers upon network formation. Although this increases network density, it does not significantly contribute towards further reducing average particle spacing on the network; moreover, it adversely affects processing performance and mechanical properties of the piezoresistive composite material [26-29].

Through innovative preparation methods, this article replaces the "self-assembly" method with the "space-restricted forced assembly (SCFNA) [28]" method for constructing the filler network, as depicted in Fig. 1. (a). The core of this approach (SCFNA) lies in achieving spatially confined extrusion and interface micro/nanomechanical assembly of the polymer micro-nano filler blend system through mechanical means, resulting in a densely conductive network with micro fillers serving as the framework and nanofillers filling the gaps within the matrix. Its advantages are as follows: it fulfills material performance requirements with lower filler content while significantly improving relevant properties under unchanged formulations. Moreover, by utilizing a structured mold array to selectively exclude volume occupied by microfilters, as illustrated in Fig. 1. (b), predominantly nanofillers enter into the pressure-sensitive unit of the microstructure, endowing it with excellent flexibility and moderate conductivity. This provides high piezoresistive response characteristics and sensitivity to the sensor. The non-pressure-sensitive area featuring a forced assembly-based conductive network ensures sufficiently high conductivity for reliable sensing capabilities. By combining both space-restricted forced assembly and volume exclusion methods, continuous integration of sensor material preparation can be achieved at low cost and high efficiency by simply replacing hot embossing flat plate molds with microstructure molds. Simultaneously, it enhances sensor performance.

II. EXPERIMENT

A. *Materials and Equipment:*

The matrix material employed is Thermoplastic Polyurethanes (TPU), specifically grade number 1170A, manufactured by BASF in Germany, with a density of 1.2g/cm^3. The short carbon fiber (SCF) utilized is grade number 10011 and produced by Toray Industries in Japan, featuring a length of 3mm. The carbon nanotubes (CNT) employed are grade number CP6092 and are manufactured by LG in South Korea. The injection molding machine model used is MA4700II2950, provided by Haitian Plastics Machinery Group Co., Ltd. The extruder model utilized is 220922B, manufactured by Nanjing Chuangbo Machinery Equipment Co., Ltd. The vacuum drying oven model employed is DZF, produced by Shanghai Lichen Bangxi Instrument Co., Ltd.

B. Sensor Preparation

To enhance dispersion and mixing, the nanocomposites were prepared following the procedure depicted in Fig. 2. (c). Taking TPU/SCF-CNT as an example, CNTs were dispersed in anhydrous ethanol and sonicated for 10 minutes. Subsequently, TPU particles were thoroughly mixed with the CNT ethanol suspension. Under ambient conditions, continuous stirring and evaporation of the solvent resulted in TPU particles uniformly coated with adhered CNT particles on their surfaces. Micron-sized conductive carbon fibers were introduced into the mixture, which was then melt-blended using an extruder to obtain a well-dispersed TPU/SCF-CNT nanocomposite particle. To eliminate moisture influence on subsequent experiments, the fabricated material was dried at 80℃ for 4 hours in a vacuum drying oven. Finally, sensor fabrication was carried out using an injection molding machine as illustrated in Fig. 2. (a), to form a microneedle array. The shape of the microneedle is conical, and the shape of the microneedle is described by the height of the cone and the diameter of the bottom surface. During the experiment, the microneedle height and bottom diameter were controlled by controlling the size of the mold. The height and bottom diameter of the injection mold used in the experiment were H_1=560um, D_1=300um; H_2=500um, D_2=580um; H_3=450um, D_3=300um; H_4=450um, D_4=580um; respectively. In addition, the center distance between the microneedles is 1mm.The injection molding machine's moving platen exerted progressive compression action in two stages: firstly from time 0 to T_1 (duration:3-50s; travel distance of moving platen:5-15mm;speed:0.1-5mm/s), followed by pressure holding stage from T_1 to T_2 (duration:0-20s) where the moving platen remained stationary, and lastly during time T_2 to T_3 (duration:0.5-5s; travel distance of moving platen:0.5-5mm; speed:0.1-10mm/s) a second compression action occurred. Cooling under pressure was applied to solidify the mold material during this process step. The in-house designed injection mold used is shown in Fig. 2. (b).

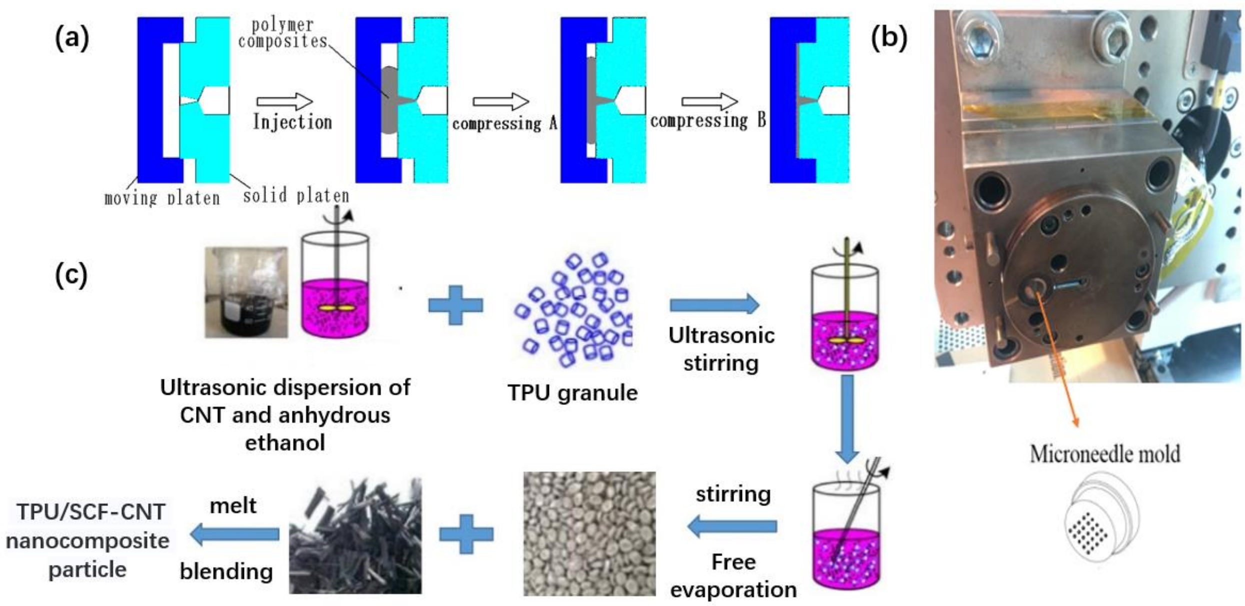

Fig. 2. (a) Process flow of injection molding machine (b) sensor (microneedles) injection mold (c) preparation process of nanocomposite materials

C. Characterization

The distribution of carbon fibers and carbon nanotubes in the microneedle array sensor was observed using a scanning electron microscope (SEM) (model S-2500CX, manufactured by Hitachi Ltd.). The integrity of the prepared microneedles was assessed by comparing their dimensions with those of the mold. The three-dimensional arrangement of the microneedles and surface roughness of the sensor were examined using laser confocal microscopy (LSCM) (model NS3600, manufactured by Shanghai Junna Technology Co., Ltd.). Fig. 3. (b) illustrates the operational principle of the sensor. A constant voltage is applied to the sensor, enabling current flow through the microneedle tips to reach the substrate. Each microstructure tip functions as a parallel resistor, as depicted in Fig. 3. (c). To ensure uniform force application during testing, a microscope cover glass was placed on top of the sensor, as shown in Fig. 3. (a). The dynamic response and sensitivity of the sensor were evaluated utilizing a pressure sensor performance testing platform (provided by Hefei Xiongqiang Numerical Control Technology Co., Ltd.).Direct current (DC) electrical conductivities of the TPU/SCF composites with higher conductivities than 10^{-6} S m^{-1} were measured by Keithley 4200-SCS (America) with a standard four probe method, while electrical conductivities of the TPU/SCF composites with lower conductivities than 10^{-6} S m^{-1} were measured by a ZC-90D resistivity meter from Shanghai Taiou Electronics (China).

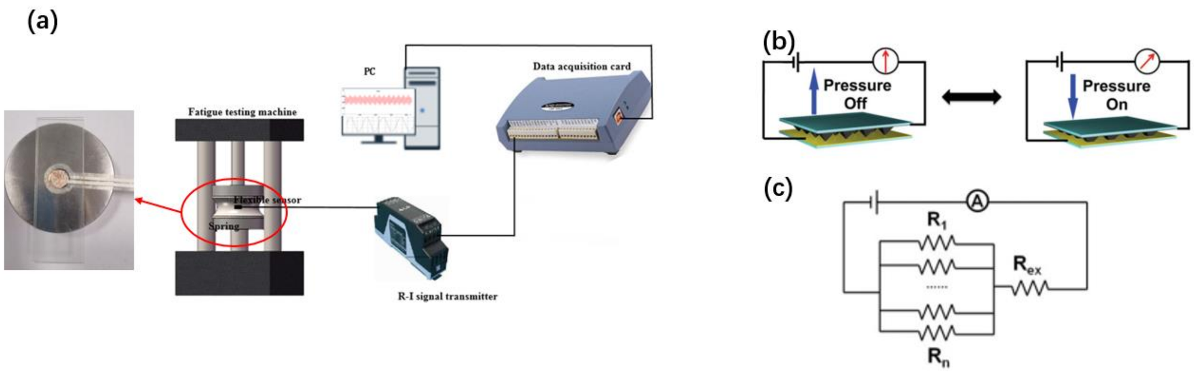

Fig. 3. (a) Sensor test platform (b) Sensor working diagram (c) Sensor working principle

III. Results and discussion

A. Sensor microstructure analysis

The performance of flexible sensors is significantly influenced by the uniform arrangement of the microneedle array. A uniform arrangement can enhance sensor sensitivity and response speed by maintaining overall balance and stability, thereby avoiding excessive or insufficient force on individual microneedle sensors within the array. Additionally, a uniform arrangement improves sensor reliability and repeatability as it ensures consistent response characteristics among different sensors. Therefore, when designing microstructure arrays for flexible sensors, particular attention should be given to achieving uniformity to maximize sensor performance. The uniform arrangement of the microneedle array was observed using LSCM. Fig. 4. (a) demonstrates the fabricated microstructures exhibiting a uniform and orderly array arrangement, which can be attributed to the mold's uniformity. The arrangement of microneedles is dependent on the fabrication mold, which can be adjusted according to specific requirements. In addition to good uniformity, smooth surfaces are essential for high-performance pressure-sensitive resistor sensors as they ensure stability and reliability while improving accuracy, responsiveness, adhesion, repeatability, and mechanical stability. The surface roughness of the microneedles observed under LSCM can be visualized in Fig. 4. (b), indicating the presence of a smooth surface on the fabricated microstructures. This is attributed to the utilization of a mold with low surface roughness.

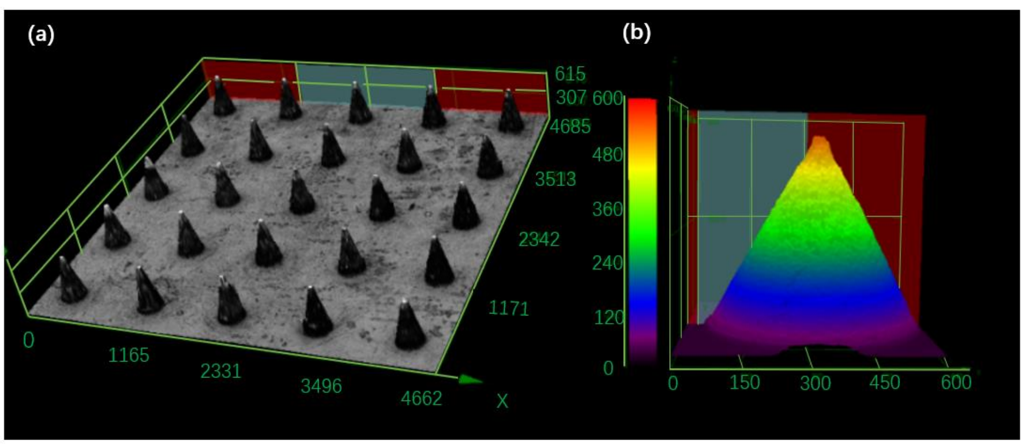

Fig. 4. (a) Microstructure arrangement under LSCM (b) Microstructure roughness under LSCM

The space-confined forced assembly method is an important step to enhance the conductivity of the sensor substrate. To verify its importance in this experiment, we prepared the test sample by changing the mold (sample size $160mm \times 80mm \times 150um$). Fig. 5. (c) and 5. (d) show the electron microscopic images of the test samples prepared by the self-assembly method and the space-confined forced assembly method, respectively. It can be clearly seen that the samples forcibly assembled using spatial limitations have a tighter SCF distribution than the samples prepared using the self-assembly method. To further verify the effect of tight SCF distribution on sensor performance, we performed conductivity tests. Fig. 5. (e) shows the conductivity test results of SCF with different contents when using spatial confined forced assembly method and self-assembly method. The results show that the conductivity of the composites increases with the increase of SCF filler content, but the composites prepared by the space-confined forced assembly method have better conductivity. This means that we can achieve higher conductivity with fewer fillers, and when the SCF filler ratio is

3.5wt%, the spatially confined forced assembly method is 10 times better than the self-assembly method. The difference of the above results is mainly due to the fact that the spatial confined forced assembly method can form a dense and continuous conductive network in the polymer material. This result is also reflected in the final sensor sample. As shown in Fig. 5. (a) and 5. (b), when the SCF filler ratio is 3.5wt%, a tight arrangement forming a network structure can be observed in the sensor base. This is similar to the results of the space-confined forced assembly verification experiment, indicating that the method does play a key role in the preparation of microstructured sensors.

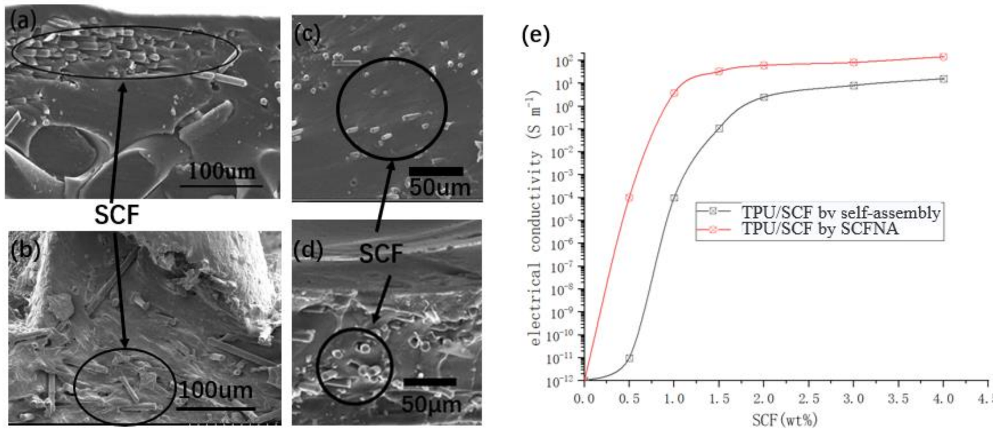

Fig. 5. (a) SEM image of SCF distribution in the substrate (b) SEM image of SCF distribution at the boundary between substrate and microneedle structure (c) SEM image of SCF distribution in composite materials prepared by self-assembly method (d) SEM image of SCF distribution in composite materials prepared by SCFNA (e) The conductivity of composites with different contents prepared by SCFNA and self-assembly methods in space confined domain.

The SEM image of the sensor in Fig. 6. (a) demonstrates a well-structured array, indicating successful fabrication. The well-organized arrangement of microneedles in Figure 6 is evident, showcasing dimensions of 500μm in height, 300μm in base diameter, and a center-to-center distance of 1mm between microneedles. Importantly, these precise dimensions align perfectly with the specifications outlined in the mold design. In Fig. 6. (b), the SEM image of the substrate reveals a tightly interconnected conductive network formed between SCF and CNT under spatial confinement-induced assembly, resulting in enhanced conductivity. Fig. 6. (c) and 6. (d) illustrate CNT within the substrate and microstructure unit respectively. A comparison shows that, apart from the TPU matrix, only CNT are present at the tip of the microstructure, suggesting that the volume exclusion method plays an essential role in ensuring predominantly nanoscale filling material within the microstructure. Consequently, superior conductivity is exhibited by the microstructure compared to the substrate. By combining spatial confinement-induced assembly with the volume exclusion method, high sensitivity can be achieved while maintaining excellent mechanical performance for this sensor design. Fig. 6. (e) indicates a small number of carbon fibers entering into the interface between the microneedle and substrate due to a larger volume of SCF compared to CNT during the volume exclusion process.

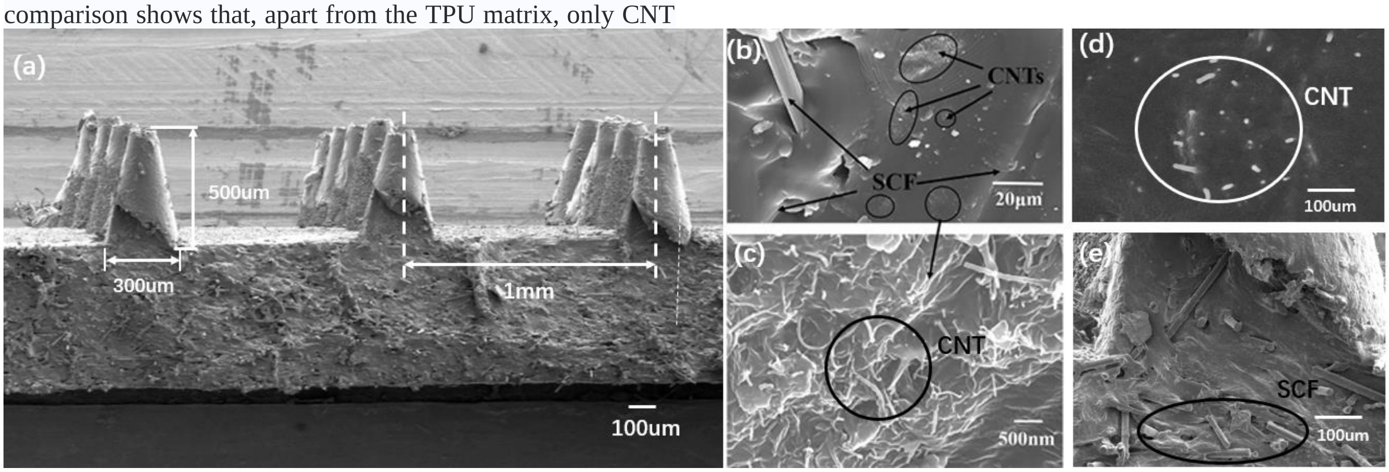

Fig. 6. (a) Microstructure arrangement under SEM (b) Distribution of SCF and CNT in the substrate (c) Distribution of CNT in the substrate (d) Distribution of CNT in the microstructure (e) distribution of SCF and CNT in the critical surface.

B. The Influence of Injection Speed and Mold Temperature on the Shape of Micro-Needle Array

Microneedles are key components of the piezoresistive sensors and act as a strain-type piezoresistive unit when using a piezoresistive sensor. The compression change of the microneedle will affect the resistance change of the sensor, thereby affecting the sensitivity of the sensor. Different micro-needle shapes will have different effects on the sensitivity of the sensor, and a precisely shaped microneedle can greatly improve the sensitivity of the sensor. To find suitable processing conditions and prepare a precisely shaped piezoresistive unit, the influence of different materials on the height of the micro-needle tip under different rotational speeds, temperatures, and mold conditions was studied. To observe the influence of external conditions on the microneedle unit more intuitively, the prepared microstructure unit was placed under an SEM for observation, and the filling percentage of the material was calculated by comparing it with the microneedle volume in the mold. Fig. 7. (a) shows the effect of different mould temperatures and extrusion speeds on the height of the microstructures using a sharp microneedle mould (mould bottom diameter D: 300 um, height H:450 um), and the error in the figure is the average height obtained from several experiments. when the injection speed is set at 300mm/s, the height of the TPU microstructure for a mold at 50°C is approximately 8% higher than that under a mold at 35°C. Moreover, for identical mold temperatures, the TPU microstructure fabricated with high extrusion speed(700mm/s) surpasses its counterpart produced with low extrusion speed(100mm/s) by about 6.7%. Notably, the piezoresistive sensor microneedles feature a sharper and more pronounced tip which leads to significant resistance changes during operation, ultimately resulting in enhanced sensitivity of the fabricated sensor. Fig. 7. (b) shows the effect of different die temperatures and extrusion speeds on the height of the microstructures using a fat microneedle die (die bottom diameter D: 580 um, height H: 450 um), and the error in the figure is the average height obtained from several experiments. The results are consistent with the use of concealed moulds, and the microstructures prepared at high mould temperature and high extrusion speed have higher heights, which is more conducive to improving the performance of the sensors. In order to investigate the effect of different die sizes on the geometry of the microneedles, the study was carried out using different shaped dies at the same die temperature and extrusion speed, and the results are shown in Fig. 7. (c). The microstructures presented in the figures were obtained using two distinct molds. The filling rate of TPU prepared with a sharp mold is superior. Under identical temperature and rotational speed conditions (50°C,500mm/s), the filling rate of TPU achieved with a sharp mold reaches 96%, which is 9% higher than that attained with a fat mold for TPU-SCF(5Vol%)-CNT(2Vol%) preparation. The higher filling ratio of the material in the mold indicates an increased presence of conductive nanomaterials within the microstructure unit, thereby positively impacting sensor sensitivity. However, it is important to note that sensor sensitivity is influenced by multiple factors and cannot be solely determined by the filling ratio of the material alone. In conclusion, enhanced injection speed and elevated mold temperature contribute to the preparation of superior micro-needle array samples.

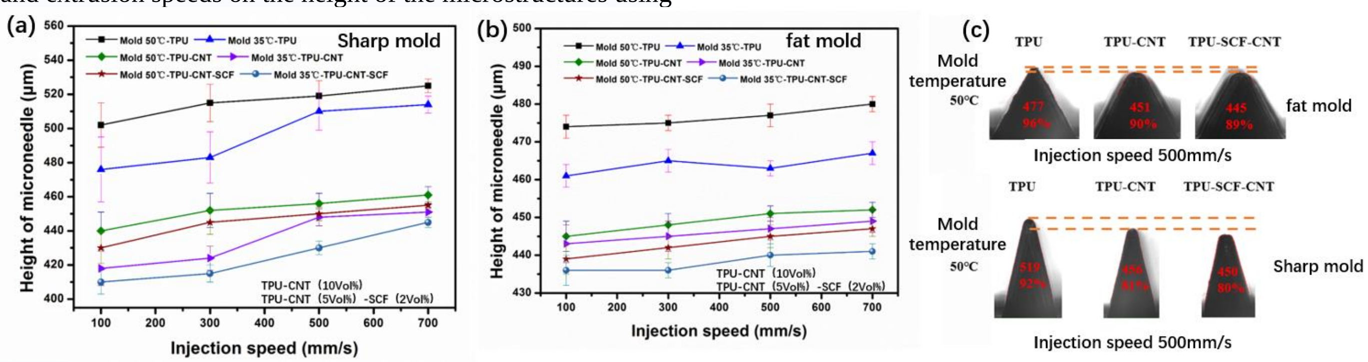

Fig. 7. (a) Microstructure heights prepared under different conditions under sharp molds (b) Microstructure heights prepared under different conditions under fat molds (c) Filling rates of microstructure prepared by different molds under the same conditions

C. *Influence of Different Sizes of Microneedle Array Shape on TPU Sensor Performance*

The sensitivity of pressure-sensitive sensors can be influenced by the size of the microneedle structure; therefore, it is imperative to investigate the impact of varying sizes of microneedle structures on sensor performance. We conducted a comprehensive analysis to examine how different-sized pressure-sensitive units affect sensor performance. The microneedle structures in Fig. 8. (a) were fabricated with varying shapes, including a sharp (H450um, D300 um) and a fat (H450 um, D580 um). The variables H and D denote the height and base diameter of the microneedle, respectively. These fabricated sensors of different sizes were tested using an in-house detection device. By subjecting the sensors to continuous pressure and observing the resulting changes in the flow of relative current, the performance of the sensors could be evaluated. The slope of the curve in Fig. 8. (b) reflects the sensor's sensitivity. The curve in the graph was fitted using the straight line difference method in the origin software to find the sensitivity of the sensor. The microneedle structure plays a pivotal role in enhancing sensor performance, as indicated by an increase in sensitivity from $0.14KPa^{-1}$ to $1.96KPa^{-1}$ for sensors with fat structures, representing a remarkable fourteen-fold improvement compared to those without microneedles. Furthermore, sensors with sharp needles exhibit enhanced sensitivity, with an increase from $1.96KPa^{-1}$ to $3.72KPa^{-1}$, resulting in a doubling of sensitivity compared to sensors with fat needles. Although Fig. 7. (c) demonstrates that microneedle structures with fat needles have higher filling rates, the results indicate that those with sharp needles exhibit greater sensitivity. This is because, under identical pressure variations, sensors featuring sharp structures undergo more significant deformation and resistance changes than their counterparts with fat structures, resulting in heightened sensitivity. The sensitivity of the sensor fabricated using the volume exclusion method and spatial confinement-induced assembly approach (TPU-SCF (5Vol%)-CNT (2Vol%)) was determined to be $4.71KPa^{-1}$. The results show that the sensor prepared using the volume exclusion method and spatial confinement-induced assembly method has a 26.6% higher sensitivity than the sensor with sharp structure and a 140% higher sensitivity than the sensor with fat structure. This is because when nano-scaled CNT is added to TPU-SCF, the microneedle structure of the mold exhibits volume exclusion effects on micro-scale fillers and nano-scale fillers, allowing nano-scale highly conductive CNT to enter the microneedle while the micro-scale SCF remains in the base. When subjected to external pressure variations, the highly conductive nanomaterial induces sensitive changes in current, which are subsequently transmitted to the ammeter through a base containing micro-scale fillers. This not only enhances the sensor's sensitivity but also improves the mechanical and conductive performance of the base, thereby significantly augmenting overall sensor sensitivity. Furthermore, Fig. 8. (b) demonstrates that the fabricated sensors exhibit a linear relationship between current and pressure under continuous pressure enhancement, satisfying the requisite linearity characteristic of this sensor.

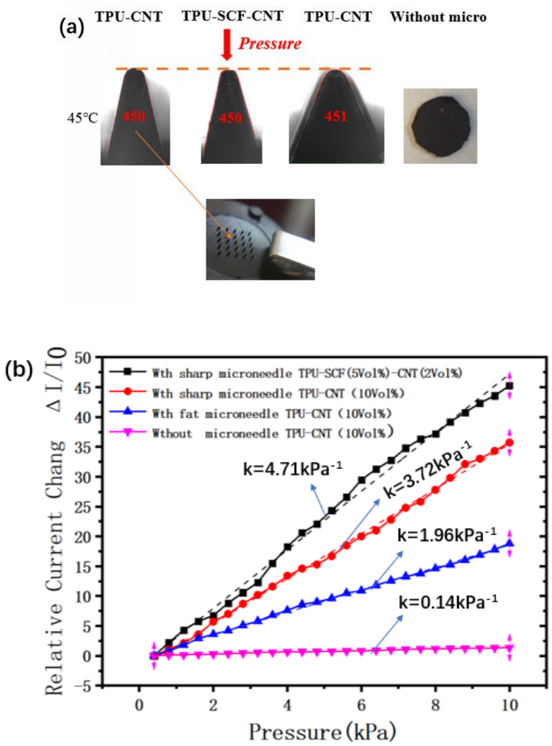

Fig. 8. (a) Comparison of microstructures of different sizes (b) Comparison of sensitivity of microstructures of different sizes

D. Sensor performance test

The dynamic mechanical response characteristics are of significant importance for the performance evaluation, selection, and application of sensors, ensuring accurate and stable measurement and detection under various dynamic working conditions. Fig. 9. illustrates the dynamic mechanical response test conducted on the sensor prepared using the volume exclusion method and spatial confinement forced assembly method. The figure demonstrates that a rapid change in a signal can be observed at the signal-receiving end when a periodic force is applied to the sensor due to its faster response time. Additionally, it is observed that the resistance change curve of the sensor closely aligns with the applied periodic force. When subjecting the sensor to a periodic force ranging from 10-60KN, corresponding changes in resistance from 310-600Ω indicate high sensitivity and accuracy.

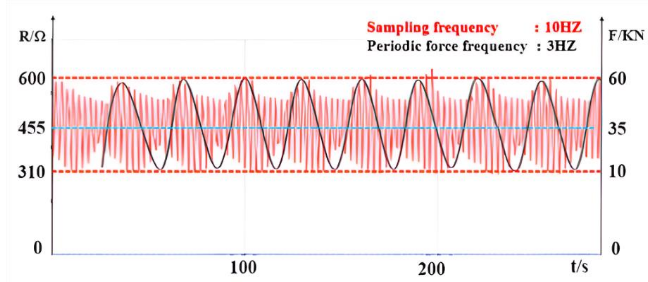

Fig. 9. Dynamic response curve of the sensor

To evaluate the sensor's performance, a force of 30KN is applied to the sensor at a frequency of 0.25HZ for an extended period of repeated loading and unloading cycle experiment in order to measure the stability and corresponding time of the sensor. As depicted in the Fig. 10. (a) and 10. (b), when subjected to external force changes, the resistance of the sensor increases rapidly; upon unloading, the sensor's resistance quickly returns to its initial state. By comparing the resistance changes of the sensor, it can be observed that the relative resistance changes in both early and late stages are essentially identical, indicating that the sensor maintains a good conductive network and exhibits strong stability after multiple loading and unloading cycles. The response time of a sensor determines its speed from perception to feedback. A fast response time ensures that environmental changes are promptly detected by the sensor, thereby enhancing its reliability and performance. As illustrated in the Fig. 10. (c), both corresponding time and recovery time of the sensor are measured at 98ms/95ms and 105ms/102ms respectively, indicating a rapid corresponding time. This is attributed to regular microstructure arrangement and excellent electrical conductivity exhibited by our prepared sensors.

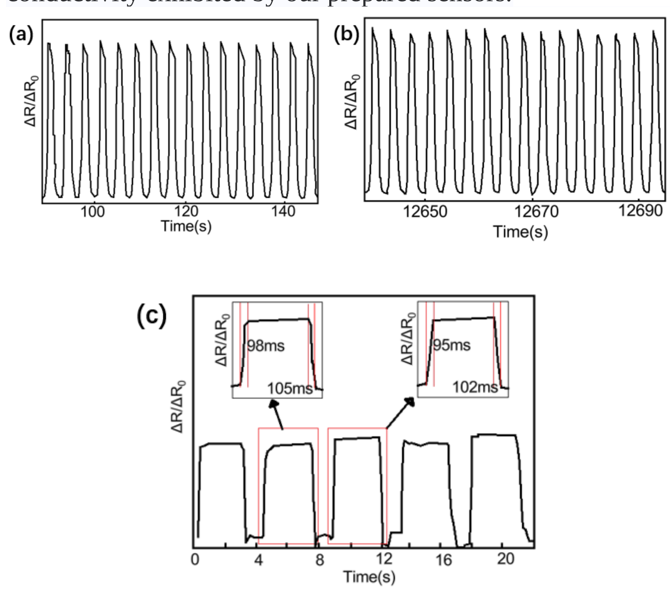

Fig. 10. (a) Preliminary repetitive test period (b) Repetitive test period (c) Sensor response time

E. Application of Sensors

Fig. 11. (e) shows the prepared sample of the sensor. In order to investigate how well the sensors can be used in reality, we will use the sensors to detect the beating of a person's pulse. As shown in Fig. 11f, three sensors are placed sequentially at three different pulse point locations, which are used to simulate a Chinese medicine practitioner taking a patient's pulse. The pulse points 1, 2 and 3 correspond to the three organs of the heart, liver and lungs of a person, and the patient's physical state can be analyzed by applying different pressures to the pulse points. Fig. 11. (a) shows the result of applying different sizes of pressure (the exact size of the pressure is uncertain) with a finger to the pulse point 1 individually and sequentially, and the sensor can clearly show the shape of the peak of the output signal of the pulsation under different pressures, which contains the main wave peak and the secondary wave peak. As the pressure continues to increase, the resistance of the sensor becomes larger, and therefore the voltage passing through the sensor also becomes larger. The doctor determines the health of the patient's heart by the pattern of the pulsations at different pressures in Figure 11a. The result of applying high pressure to the pulse points 1, 2 and 3 is shown in Fig. 11. (b) (c) (d), it can be clearly found that the voltage of pulse point 1 is the highest, the other two voltages are close to each other, meanwhile the beating of all three pulse points are smooth, which indicates that the tester is in good health. These results show that the sensor is capable of detecting the tiny beating signals of the veins and exhibits properties such as high sensitivity and fast response time. The potential application of the sensor for wearable technology is illustrated.

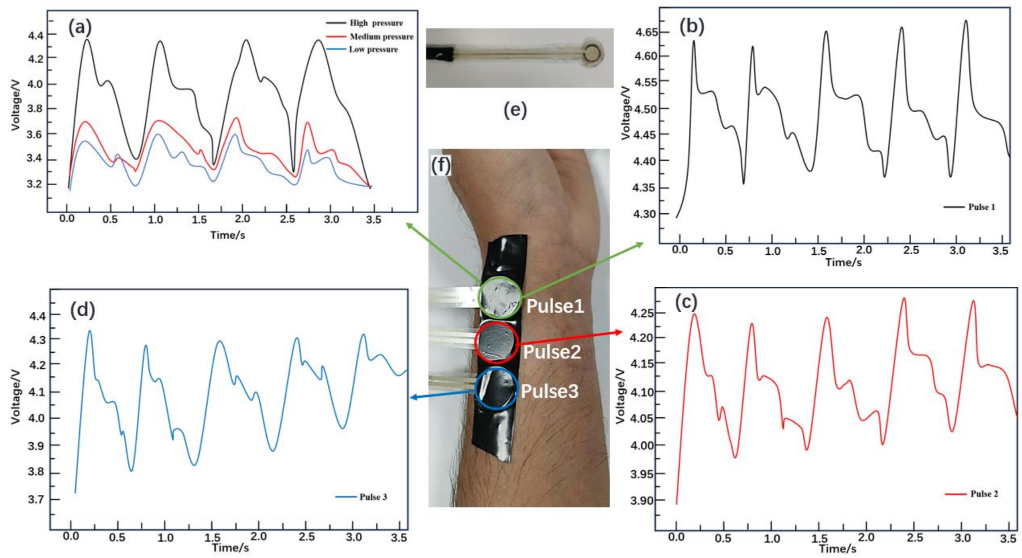

Fig. 11. (a) Signal output of pulse point 1 at different pressures (b) Signal output of pulse 1 at high pressure (c) Signal output of pulse 2 at high pressure (d) Signal output of pulse 3 at high pressure (e) Pulse diagnosis test platform

IV. Conclusion

This study successfully demonstrates the advantages of using volume exclusion and spatial confinement forced assembly methods in fabricating microneedle sensors. These innovative preparation techniques result in microneedles with predominantly nanoscale fillers, leading to significantly enhanced electrical conductivity and increased sensitivity. Specifically, the spatial confinement forced assembly method produces a tightly packed filler network, which not only improves the mechanical performance of the substrate but also maintains moderate electrical conductivity.

The sensors prepared high extrusion speed and elevated mold temperature under conditions exhibit superior quality, with large aspect ratios contributing to enhanced sensitivity. Notably, the sensors fabricated using these advanced methods show a 26.6% improvement in sensitivity for large aspect ratios, a remarkable 140% enhancement compared to sensors with small aspect ratios. Furthermore, these methods offer faster response times and greater accuracy than conventional fabrication techniques.

Beyond these performance improvements, the adaptability of these methods allows for the production of customized sensors tailored to specific needs by simply adjusting the mold size. By integrating spatial confinement forced assembly with volume exclusion, it is possible to replace traditional hot-press flat molds with a microneedle mold, enabling continuous, cost-effective, and efficient sensor production.

In summary, these advanced fabrication techniques not only enhance sensor performance but also pave the way for the scalable and customizable production of high-performance sensors.

V. References

[1] Lee B, Kim J, Kim H, et al. Low-cost flexible pressure sensor based on dielectric elastomer film with micro-pores[J]. Sensors Actuators: A. Physical,2016,240103-109.

[2] Zhang P, Chen Y, Li Y, et al. Flexible Piezoresistive Sensor with the Microarray Structure Based on Self-Assembly of Multi-Walled Carbon Nanotubes[J]. Sensors,2019,19(22):4985-4985.

[3] Shi X, Zhang S, Chen X, et al. Three-dimensional

graphene/carbonized metal-organic frameworks based high-performance supercapacitor[J]. Carbon,2020,157(C):55-63.

[4] Shu Yi. Basic Research of Flexible Pressure Sensor Based on Novel Micro-Nano Structure [D]. Tsinghua University, 2015.

[5] Cui J, Zhang B, Duan J, et al. Flexible Pressure Sensor with Ag Wrinkled Electrodes Based on PDMS Substrate[J]. Sensors,2016,16(12):2131.

[6] Cheng-Hui L, Chao W, Christoph K, et al. A highly stretchable autonomous self-healing elastomer. [J]. Nature Chemistry,2016,8(6):618-24.

[7] Tang Z, Wang Z, Lu J, et al. Design of robot finger based on flexible tactile sensor[J]. International Journal of Advanced Robotic Systems,2019,16(5):1729881419879853-1729881419879853.

[8] ZHU B, LING Y, YAP L W, et al. Hierarchically structure d vertical gold nanowire array-based wearable pressure se nsors for wireless health monitoring [J]. ACS Applied Mat erials & Interfaces, 2019, 11 (32): 29014-29021.

[9] NIU H, GAO S, YUE W, et al. Highly morphology contr ollable and highly sensitive capacitive tactile sensor based on epidermis-dermis-inspired interlocked asymmetric-na nocone arrays for detection of tiny pressure[J]. Small, 202 0, 16(4): 1904774.

[10] CHEN W, GUI X, LIANG B, et al. Structural engineering for high sensitivity, ultrathin pressure sensors based on wrinkled graphene and anodic aluminum oxide membrane [J]. ACS Applied Materials & Interfaces, 2017, 9(28): 241 11-24117.

[11] GUO Y, GAO S, YUE W, et al. Anodized aluminum oxide -assisted low-cost flexible capacitive pressure sensors bas ed on double-sided nanopillars by a facile fabrication met hod[J]. ACS Applied Materials & Interfaces, 2019, 11(51): 48594-48603.

[12] WAN Y, QIU Z, HONG Y, et al. A highly sensitive flexibl e capacitive tactile sensor with sparse and high-aspect-rati o microstructures[J]. Advanced Electronic Materials, 201 8, 4(4): 1700586.

[13] WEI Y, CHEN S, LIN Y, et al. Cu-Ag core-shell nanowire s for electronic skin with a petal molded microstructure [J]. Journal of Materials Chemistry C, 2015, 3(37): 9594-960 2.

[14] ZHOU Q, JI B, WEI Y, et al. A bio-inspired cilia array as the dielectric layer for flexible capacitive pressure sensors with high sensitivity and a broad detection range[J]. Jour nal of Materials Chemistry A, 2019, 7(48): 27334-27346.

[15] JI B, ZHOU Q, HU B, et al. Bio-inspired hybrid dielectric for capacitive and triboelectric tactile sensors with high s ensitivity and ultrawide linearity range [J]. Advance Mate rials, 2021, 33(27): 2100859.

[16] Hu Y, Wang Z, et al. Efficient concentration of trace analy te with ordered hotspot construction for a robust and sensi tive SERS platform[J]. International Journal of Extreme Manufacturing, 2024, 6(3): 035505.

[17] Qi Shao, et al., High-Performance and Tailorable Pressure Sensor Based on Ultrathin Conductive Polymer Film[J], Small, 2014, 10(8), 1466-1472.

[18] Xiaolong Gao, Wu DM, et al., Improved Electrical Conductivity of PDMS/SCF Composite sheets with Bolting Cloth Prepared by a Spatial Confining Forced Network Assembly method[J]. RSC Advances, 2017, 7, 14761 - 14768.

[19] Xiaolong Gao, and Daming Wu. Mechanically Enhanced Electrical Conductivity of Polydimethylsiloxane-Based Composites by a Hot Embossing Process[J]. Polymers, 2019, 11,56.

[20] Zewen Yang, Hong Xu, Xiaolong Gao, et al., Measuring mechanism and applications of polymer-based flexible sensors[J]. Sensors, 2019, 1(19).

[21] Zhu J, Wei S, Ryu J, et al. In situ stabilized carbon nanofiber (CNF) reinforced epoxy nanocomposites[J]. Journal of Materials Chemistry, 2010, 20(23): 4937-4948.

[22] Liu H, Gao J, Huang W, et al. Electrically conductive strain sensing polyurethane nanocomposites with synergistic carbon nanotubes and graphene bifillers [J]. Nanoscale, 2016, 8(26): 12977-12989.

[23] Zhang X, Yan X, He Q, et al. Electrically conductive polypropylene nanocomposites with negative permittivity at low carbon nanotube loading levels[J]. ACS applied materials & interfaces, 2015, 7(11): 6125-6138

[24] Zhang K, Yu H O, Shi Y D, et al. Morphological regulation improved electrical conductivity and electromagnetic interference shielding in poly (l-lactide)/poly (ε-caprolactone)/carbon nanotube nanocomposites via constructing stereocomplex crystallites[J]. Journal of Materials Chemistry C, 2017, 5(11): 2807-2817.

[25] Gong T, Liu MQ, Liu H, et al. Selective distribution and migration of carbon nanotubes enhanced electrical and mechanical performances in polyolefin elastomers[J]. Polymer, 2017, 110: 1-11.

[26] Socher R, Krause B, Müller MT, Boldt R and Pötschke P. The influence of matrix viscosity on MWCNT dispersion and electrical properties in different thermoplastic nanocomposites[J]. Polymer, 2012, 53(2): 495-504.

[27] Ranvijai R, Rahaman M, Khastgir D. Electrical properties of polyvinylidene fluoride (PVDF)/multi-walled carbon nanotube (MWCNT) semi-transparent composites: Modelling of DC conductivity[J]. Composites Part A, 2015, 69:30-39.

[28] Yang BJ, Jang J, Eem SH, Kim SY. A probabilistic micromechanical modeling for electrical properties of nanocomposites with multi-walled carbon nanotube morphology[J]. Composites Part A, 2017, 92:108-117.

[29] Park OK, Lee W, Hwang JY, et al. Mechanical and electrical properties of thermochemically cross-linked polymer carbon nanotube fibers[J]. Composites Part A, 2016, 91:222-228

[30] Pan L, Bao Z, et al., An ultra-sensitive resistive pressure sensor based on hollow-sphere microstructure induced elasticity in conducting polymer film[J]. Nat.Commun., 2014, 5, 3002.